

The geometry of reaction trajectories and attracting manifolds in composition space

ZHUYIN REN* and STEPHEN B. POPE

Sibley School of Mechanical & Aerospace Engineering Cornell University, Ithaca, NY 14853, USA

(Received 17 March 2005; in final form 21 October 2005)

In numerical simulations of combustion processes, the use of dimension reduction to simplify the description of the chemical system has the advantage of reducing the computational cost, but it is important also to retain accuracy and adequate detail. Most existing dimension reduction methods assume the existence of low-dimensional attracting manifolds in the full composition space and try to approximate or directly identify the low-dimensional attracting manifolds. However, questions remain about the geometry of the reaction trajectories in the full composition space, the existence of the low-dimensional attracting manifolds in low-temperature regions, and the minimum dimension of the attracting manifold required for describing a particular chemical system. This paper tries to address some of these issues by studying the reaction trajectories starting from a wide range of different initial compositions for both H₂/air and CH₄/air mixtures. Along each trajectory, we study the tangent bundle of the trajectory, the eigenvalues of the Jacobian matrices, and the singular values of the sensitivity matrices (i.e. sensitivity with respect to initial composition). It is shown that the dimension of the affine space containing a trajectory (or of the tangent bundle along a trajectory) is much smaller than the dimension of the full composition space. Even at low temperatures, the Jacobian matrices still have a significant number of large (in magnitude) negative eigenvalues, which implies the existence of fast time scales and low-dimensional attracting manifolds (even at low temperatures). The geometrical significance of sensitivity matrices is explored. Based on the sensitivity matrices, a new method is proposed to determine the minimum dimension of the attracting manifold required for describing a chemical system with prescribed accuracy, and to identify the ‘principal subspace’ which is an approximation to the tangent space of the attracting manifold.

Keywords: Dimension reduction; Attracting manifold; Reduced chemistry

Nomenclature

$d_\epsilon(t)$	dimension of the attracting manifold along reaction trajectories
n_e	number of elements
n_s	number of species
n_r	dimension of reduced composition
n_ϕ	dimension of full composition
$n_\mathcal{E}$	dimension of the conserved subspace
$n_\mathcal{R}$	dimension of the reactive subspace

*Corresponding author. E-mail: zr26@cornell.edu

$n'_{\mathcal{R}}$	dimension of the affine space containing individual trajectory
\mathbf{r}	reduced composition
\mathbf{A}	sensitivity matrix
$\mathbf{A}^{\mathcal{R},\mathcal{R}}$	sensitivity matrix corresponding to the reactive subspace in the $\hat{\mathbf{C}} - \mathbf{W}$ basis
\mathcal{C}	full composition space
\mathcal{E}	conserved subspace
\mathcal{R}	reactive subspace
\mathbf{e}_i	canonical basis vector for composition space, $i = 1, 2, \dots, n_{\phi}$
$\hat{\mathbf{C}}$	matrix whose columns form an orthonormal basis for \mathcal{E}
\mathbf{W}	matrix whose columns form an orthonormal basis for \mathcal{R}
\mathbf{J}	Jacobian matrix
$\mathbf{R}(\phi^0, t)$	reaction mapping
$\mathbf{R}^{\mathcal{E}}$	component of \mathbf{R} in the conserved subspace
$\mathbf{R}^{\mathcal{R}}$	component of \mathbf{R} in the reactive subspace
\mathbf{S}	the rate of change of composition
$\mathbf{S}^{\mathcal{E}}$	component of \mathbf{S} in the conserved subspace
$\mathbf{S}^{\mathcal{R}}$	component of \mathbf{S} in the reactive subspace
\mathbf{T}	unit tangent vector along the trajectory
$\bar{\mathbf{T}}$	tangent bundle matrix
κ	curvature
λ_i	eigenvalues of \mathbf{J} , $i = 1, 2, \dots, n_{\phi}$
λ_i^r	real part of eigenvalues, $i = 1, 2, \dots, n_{\phi}$
σ_i	singular values of the matrix \mathbf{A} , $i = 1, 2, \dots, n_{\phi}$
$\hat{\sigma}_i$	singular values of $\mathbf{A}^{\mathcal{R},\mathcal{R}}$, $i = 1, 2, \dots, n_{\mathcal{R}}$
$\bar{\sigma}_i$	singular values of $\bar{\mathbf{T}}$
$\sigma_i^>$	singular values of matrix $\mathbf{A}^{\mathcal{R},\mathcal{R}}$ which are greater than threshold value
$\sigma_i^<$	singular values of matrix $\mathbf{A}^{\mathcal{R},\mathcal{R}}$ which are no greater than threshold value
ϕ	full composition
$\phi^{\mathcal{E}}$	component of ϕ in the conserved subspace
$\phi^{\mathcal{R}}$	component of ϕ in the reactive subspace
$\hat{\phi}^{\mathcal{E}}, \hat{\phi}^{\mathcal{R}}$	coordinates in the $\hat{\mathbf{C}} - \mathbf{W}$ basis

1. Introduction

The computational cost of using the detailed chemical information in combustion simulations can be dramatically reduced by exploiting techniques of dimension reduction [1–13]. The aim of dimension reduction strategies is to represent the chemistry accurately in terms of a relatively small number n_r of reduced composition variables $\mathbf{r} = \{r_1, r_2, \dots, r_{n_r}\}$ instead of directly in terms of the $n_{\phi} = n_s + 1$ full composition variables (species specific moles and enthalpy) $\phi = \{\phi_1, \phi_2, \dots, \phi_{n_{\phi}}\}$. Then in the combustion simulation, the relevant equations are solved for the n_r reduced compositions instead of for the n_{ϕ} full compositions.

The geometrical interpretation of the dimension reduction assumption is that the full composition is (by assumption) known in terms of the reduced composition, i.e.

$$\phi = \phi^m(\mathbf{r}), \quad (1)$$

where the function $\phi^m(\mathbf{r})$ defines an n_r -dimensional manifold parameterized by \mathbf{r} in the n_{ϕ} -dimensional full composition space.

Most of the dimension reduction methods are based on the observation that, in a typical combustion process, there is a wide range of time scales present in the chemical mechanism. The very fast time-scales are usually associated with local equilibrium or quasi-steady state, while the long-term dynamics of the combustion system are determined by a small number n_r of slow processes (at least after the decay of initial transients). Geometrically, the long term behaviour of the combustion system can be described by a finite-dimensional attractor of lower dimension than the full composition space. The attractor is embedded in an low-dimensional, invariant, smooth manifold called the invariant attracting manifold \mathcal{M}_A which locally attracts all trajectories [14]. Each existing dimension reduction method based on time-scale analysis of the combustion system assumes the existence of the n_r low-dimensional attracting manifold \mathcal{M}_A in the full composition space and constructs an n_r -dimensional manifold to directly identify or approximate it.

Questions remain concerning the geometry of the trajectories in composition space, the existence of low dimensional attracting manifolds in low-temperature regions, and the minimum dimension of the attracting manifold required for describing a particular chemical system with prescribed accuracy. Specifically:

- As shown in ref. [15], to determine the dimensionality of the accessed region in composition space (which is the union of all the compositions for all positions and times in a reactive flow), an important issue is to determine the dimensionality of the affine space containing individual reaction trajectories, i.e. the dimensionality of the tangent bundle along individual trajectories.
- It is well known that the behaviours of chemical kinetics at low temperature are significantly different than at high temperature [14]. At low temperature, the reactions are usually slow and the chemical time scales are significantly larger than at high temperature. Yet there are few direct studies of time scales in the chemical kinetics at low temperature. Direct support for the existence of low-dimensional attracting manifolds at low temperature is not available.
- For dimension reduction methods, it is essential to determine the minimum dimensionality of the attracting manifold required for a particular chemical system, and to know how fast the compositions relax to this attracting manifold. There are several existing algorithms [16–20] that determine the local dimension of the attracting manifold for chemical systems. All these methods are based on the analysis of the local Jacobian matrix and on the separation in the eigenvalue spectrum of this matrix. In this paper, after exploring the geometrical significance of the sensitivity matrices along the trajectories in the composition space, we give a criterion to determine the minimum dimension of the attracting manifold. Compared with other methods, it is based on the sensitivity matrices instead of local Jacobian matrices.

In this work, for both H_2/air and CH_4/air combustion, trajectories starting from a wide range of different initial compositions are studied. For each trajectory, we show the dimension of the affine space containing this trajectory and the eigenvalue spectrum along it. Following that, we discuss the significance of sensitivity matrices and introduce the method to determine the minimum dimension of the attracting manifold and to identify the ‘principal subspace’.

2. Tangent bundle, Jacobian matrices and sensitivity matrices

In this section we introduce the principal quantities that are investigated, and give some of their fundamental properties.

2.1 Composition space: conserved and reactive subspaces

We consider a homogeneous, adiabatic, isobaric reacting system consisting of n_s chemical species. The extension to other systems, such as a constant-volume isothermal one, is straightforward. Modelling reaction kinetics in this system usually leads to a stiff system of ordinary differential equations (ODEs). At time t , the full composition is represented by the $n_\phi = n_s + 1$ composition variables $\phi(t) \equiv \{\phi_1, \phi_2, \dots, \phi_{n_\phi}\}$, which we take to be the species specific moles and enthalpy.

The full composition space \mathcal{C} is defined to be the real n_ϕ -dimensional Euclidean space with canonical basis vectors $\mathbf{e}_k, k = 1, 2, \dots, n_\phi$ in which the first n_s directions correspond to species and the last corresponds to enthalpy. The composition space \mathcal{C} can be decomposed into the conserved subspace \mathcal{E} , and the reactive subspace \mathcal{R} (which is the orthogonal complement of \mathcal{E}). With n_e being the number of chemical elements in the system, the conserved subspace is of dimension $n_\mathcal{E} = n_e + 1$, reflecting the conservation of elements and enthalpy. The conserved subspace \mathcal{E} is the space spanned by the following $n_\phi \times n_\mathcal{E}$ matrix

$$\mathbf{C} \equiv \begin{bmatrix} \mathbf{E} & 0 \\ 0 & 1 \end{bmatrix}, \quad (2)$$

where the first n_e columns of \mathbf{C} are vectors in composition space \mathcal{C} corresponding to the elements and the last column is the canonical basis vector corresponding to enthalpy. The element matrix \mathbf{E} , whose general component is E_{kj} , is an $n_s \times n_e$ matrix with non-negative integer components, and E_{kj} denotes the number of atoms of element j in one molecule of species k . Every row of \mathbf{E} has at least one non-zero entry. The reactive subspace \mathcal{R} is the orthogonal complement of the conserved subspace and is of dimension $n_\mathcal{R} = n_\phi - n_e - 1$.

It is convenient to introduce orthonormal basis for the conserved and reactive subspaces. Thus we denote by $\hat{\mathbf{C}}$ an $n_\phi \times n_\mathcal{E}$ matrix whose orthonormal columns span \mathcal{E} ; and similarly we denote by \mathbf{W} an $n_\phi \times n_\mathcal{R}$ matrix whose orthonormal columns span \mathcal{R} . Thus the $n_\phi \times n_\phi$ matrix $[\hat{\mathbf{C}} \mathbf{W}]$ is orthonormal and its columns span the composition space \mathcal{C} . The composition ϕ (and indeed any other vector in \mathcal{C}) can be decomposed into components in the conserved ($\phi^\mathcal{E}$) and the reactive ($\phi^\mathcal{R}$) subspaces

$$\phi = \phi^\mathcal{E} + \phi^\mathcal{R} = \hat{\mathbf{C}}\hat{\phi}^\mathcal{E} + \mathbf{W}\hat{\phi}^\mathcal{R}, \quad (3)$$

where $\phi^\mathcal{E} = \hat{\mathbf{C}}\hat{\mathbf{C}}^T\phi$ and $\phi^\mathcal{R} = \mathbf{W}\mathbf{W}^T\phi$ are the components (which are independent of the chosen basis); and $\hat{\phi}^\mathcal{E} = \hat{\mathbf{C}}^T\phi$ (a vector of length $n_\mathcal{E}$) and $\hat{\phi}^\mathcal{R} = \mathbf{W}^T\phi$ (a vector of length $n_\mathcal{R}$) are the coordinates in the $\hat{\mathbf{C}} - \mathbf{W}$ basis.

Moreover all compositions that occur in the system satisfy realizability, and hence (by definition) are in the realizable region. This is defined as the $(n_\phi - 1)$ -dimensional region of the composition space corresponding to non-negative species specific moles satisfying the normalization condition and with the enthalpy corresponding to positive absolute temperatures.

2.2 Reaction mapping and trajectories

In the homogeneous adiabatic, isobaric system considered, due to the chemical reactions, the composition evolves by the autonomous ODEs

$$\frac{d\phi(t)}{dt} = \mathbf{S}(\phi(t)), \quad (4)$$

where \mathbf{S} is the rate of change of composition given by the detailed chemical kinetic mechanism, which we refer to as the rate vector. The rate vector \mathbf{S} can be decomposed into components

in the conserved and reactive subspaces, $\mathbf{S} = \mathbf{S}^{\mathcal{E}} + \mathbf{S}^{\mathcal{R}}$, but because the conserved variables (elements and enthalpy) are indeed conserved (in an adiabatic, isobaric reaction), we have $\mathbf{S}^{\mathcal{E}} = 0$.

The reaction mapping $\mathbf{R}(\phi^0, t)$ is defined to be the solution to equation (4) after time t , starting from the initial condition ϕ^0 . Thus $\mathbf{R}(\phi^0, t)$ is completely defined by the equations

$$\mathbf{R}(\phi^0, 0) = \phi^0, \quad (5)$$

and

$$\frac{\partial \mathbf{R}(\phi^0, t)}{\partial t} = \mathbf{S}(\mathbf{R}(\phi^0, t)). \quad (6)$$

For fixed ϕ^0 and t increasing from zero, in the n_{ϕ} -dimensional composition space, $\mathbf{R}(\phi^0, t)$ represents the reaction trajectory from ϕ^0 , which approaches the chemical equilibrium composition as t tends to infinity. The decomposition $\mathbf{R} = \mathbf{R}^{\mathcal{E}} + \mathbf{R}^{\mathcal{R}}$ and equations (5) and (6) yield

$$\mathbf{R}^{\mathcal{E}}(\phi^0, t) = \phi^{0,\mathcal{E}} \quad (7)$$

(i.e. the conserved component is conserved for all time); and

$$\begin{aligned} \frac{\partial \mathbf{R}^{\mathcal{R}}(\phi^0, t)}{\partial t} &= \mathbf{S}^{\mathcal{R}}(\mathbf{R}) = \mathbf{S}(\mathbf{R}) \\ &= \mathbf{S}(\phi^{0,\mathcal{E}} + \mathbf{R}^{\mathcal{R}}). \end{aligned} \quad (8)$$

Thus $\mathbf{R}^{\mathcal{R}}(\phi^0, t)$ represents the reaction trajectory in the $n_{\mathcal{R}}$ -dimensional reactive subspace, while $\mathbf{R}^{\mathcal{E}}(\phi^0, t)$ is fixed at its initial value. Therefore, during chemical reactions, due to the conservation of elements and enthalpy, the reaction trajectories are confined in the reactive subspace.

For the adiabatic, isobaric system considered, the chemical equilibrium is determined by the element composition (n_e elements) and enthalpy, i.e. the chemical equilibrium composition

$$\mathbf{R}(\phi^0, \infty) = \mathbf{R}(\phi^{0,\mathcal{E}} + \phi^{0,\mathcal{R}}, \infty) \quad (9)$$

is independent of $\phi^{0,\mathcal{R}}$.

2.3 Tangent vectors and curvature

The reaction trajectory is a curve (i.e. a one-dimensional manifold) that can be parameterized by time t , by arclength s , by entropy, or by any other quantity which varies monotonically along it. For each point along the reaction trajectory starting from ϕ^0 in the composition space, the unit tangent vector is

$$\mathbf{T}(\phi^0, t) = \frac{\mathbf{S}(\mathbf{R}(\phi^0, t))}{\|\mathbf{S}(\mathbf{R}(\phi^0, t))\|}, \quad (10)$$

where $\|\phi\|$ denotes the 2-norm $(\phi^T \phi)^{1/2}$. The tangent bundle is the collection of the unit tangent vectors at all points on this trajectory.

Along the reaction trajectory starting from ϕ^0 , the curvature κ is

$$\kappa(s) = \left\| \frac{d\mathbf{T}}{ds} \right\|, \quad (11)$$

where the trajectory is parameterized by the arclength s . Both s and κ^{-1} have units of kmol/kg.

2.4 Jacobian and sensitivity matrices

The Jacobian matrix \mathbf{J} is defined as

$$J_{ij}(\phi) \equiv \frac{\partial S_i(\phi)}{\partial \phi_j}. \quad (12)$$

Then the Jacobian \mathbf{J} along the trajectory starting from ϕ^0 is

$$\bar{J}_{ij}(\phi^0, t) = J_{ij}(\mathbf{R}(\phi^0, t)), \quad (13)$$

which reveals the chemical time scales in terms of its eigenvalues as shown in a later section.

Sensitivity analysis investigates the effect of changes in parameters on the solution of mathematical models. The application of sensitivity analysis in the field of chemical kinetics is extensively reviewed in refs [21, 22]. Here we consider the sensitivity of the reaction mapping with respect to the initial composition. The sensitivity (to initial condition) matrix $\mathbf{A}(\phi^0, t)$ is an $n_\phi \times n_\phi$ matrix defined by

$$A_{ij}(\phi^0, t) \equiv \frac{\partial R_i(\phi^0, t)}{\partial \phi_j^0}. \quad (14)$$

It is readily deduced from equation (4) that (for fixed ϕ^0) \mathbf{A} evolves according to the system of ordinary differential equations

$$\frac{d}{dt}\mathbf{A}(\phi^0, t) = \mathbf{J}(\mathbf{R}(\phi^0, t))\mathbf{A}(\phi^0, t), \quad (15)$$

from the initial condition

$$\mathbf{A}(\phi^0, 0) = \mathbf{I}. \quad (16)$$

In the computations reported below, the Jacobian is calculated by automatic differentiation using ADIFOR [23]. Compared to using divided differences, this technique makes the Jacobian calculations more robust and accurate. Equations (4) and (15) are solved together using DDASAC code [24] to obtain $\mathbf{R}(\phi^0, t)$ and $\mathbf{A}(\phi^0, t)$ given the initial composition ϕ^0 .

3. Geometrical significance of the sensitivity matrices

The sensitivity (to initial condition) matrix describes the effect of the perturbation in the initial composition on the reaction mapping. Skodje and Davis [13] even used the sensitivity matrix to construct low-dimensional manifolds in composition space. It is informative to take a geometrical view of the significance of the sensitivity matrix. Let the singular value decomposition (SVD) of \mathbf{A} be

$$\mathbf{A} = \mathbf{U}_A \Sigma_A \mathbf{V}_A^T, \quad (17)$$

where \mathbf{U}_A and \mathbf{V}_A are $n_\phi \times n_\phi$ orthogonal matrices and Σ_A is the diagonal matrix of singular values, $\sigma_1 \geq \sigma_2 \geq \dots \geq \sigma_{n_\phi} \geq 0$. The columns of \mathbf{U}_A ($\mathbf{u}_i, i = 1, 2, \dots, n_\phi$) and columns of \mathbf{V}_A ($\mathbf{v}_i, i = 1, 2, \dots, n_\phi$) are the left and right singular vectors, respectively. It is readily shown from equation (14) that the infinitesimal change in the reaction mapping, $d\mathbf{R}$, with respect to the infinitesimal perturbation in the initial composition, $d\phi^0$, can be written as

$$d\mathbf{R} = \mathbf{A}d\phi^0 = \mathbf{U}_A \Sigma_A \mathbf{V}_A^T d\phi^0. \quad (18)$$

3.1 Mapping of an infinitesimal ball in composition space

A geometrical interpretation of equation (18) is that the infinitesimal ball of radius dr centred at the initial composition ϕ^0

$$\{\phi = \phi^0 + d\phi^0 \mid \|d\phi^0\| \leq dr\} \quad (19)$$

is mapped to the hyper-ellipsoid

$$\{\phi = \mathbf{R} + d\mathbf{R} \mid \|\mathbf{A}^{-1}d\mathbf{R}\| \leq dr\}, \quad (20)$$

or, equivalently,

$$\{\phi = \mathbf{R} + d\mathbf{R} \mid \|\Sigma_A^{-1}\mathbf{U}_A^T d\mathbf{R}\| \leq dr\}, \quad (21)$$

which is centred at the reaction mapping $\mathbf{R}(\phi^0, t)$.

Hence, as shown in figure 1, the geometrical significance of the sensitivity matrix is that the initial n_ϕ -dimensional infinitesimal ball centred at the initial point ϕ^0 is mapped at time t to an n_ϕ -dimensional hyper-ellipsoid centered at $\mathbf{R}(\phi^0, t)$. The principal semi-axes are $dr\sigma_i\mathbf{u}_i$, where \mathbf{u}_i is the i th column of \mathbf{U}_A . For singular values which are greater than unity, the initial ball is elongated in the corresponding principal directions, while for singular values which are smaller than unity, the initial ball is compressed in the corresponding principal directions. The smaller the singular value, the smaller the effect of the initial perturbation in the direction of the corresponding right singular vector on the reaction mapping.

In the $\hat{\mathbf{C}} - \mathbf{W}$ basis, the sensitivity matrix has the structure

$$\begin{bmatrix} \frac{\partial \hat{\mathbf{R}}^\mathcal{E}}{\partial \hat{\phi}^{0,\mathcal{E}}} & \frac{\partial \hat{\mathbf{R}}^\mathcal{E}}{\partial \hat{\phi}^{0,\mathcal{R}}} \\ \frac{\partial \hat{\mathbf{R}}^\mathcal{R}}{\partial \hat{\phi}^{0,\mathcal{E}}} & \frac{\partial \hat{\mathbf{R}}^\mathcal{R}}{\partial \hat{\phi}^{0,\mathcal{R}}} \end{bmatrix} = \begin{bmatrix} \mathbf{I} & 0 \\ \frac{\partial \hat{\mathbf{R}}^\mathcal{R}}{\partial \hat{\phi}^{0,\mathcal{E}}} & \frac{\partial \hat{\mathbf{R}}^\mathcal{R}}{\partial \hat{\phi}^{0,\mathcal{R}}} \end{bmatrix}. \quad (22)$$

Furthermore, $d\phi^0$ and $d\mathbf{R}$ can be expressed as

$$d\phi^0 = \hat{\mathbf{C}}d\hat{\phi}^{0,\mathcal{E}} + \mathbf{W}d\hat{\phi}^{0,\mathcal{R}} \quad (23)$$

and

$$d\mathbf{R} = \hat{\mathbf{C}}d\hat{\mathbf{R}}^\mathcal{E} + \mathbf{W}d\hat{\mathbf{R}}^\mathcal{R}, \quad (24)$$

where $d\hat{\phi}^{0,\mathcal{E}} = \hat{\mathbf{C}}^T d\phi^0$, $d\hat{\phi}^{0,\mathcal{R}} = \mathbf{W}^T d\phi^0$, $d\hat{\mathbf{R}}^\mathcal{E} = \hat{\mathbf{C}}^T d\mathbf{R}$ and $d\hat{\mathbf{R}}^\mathcal{R} = \mathbf{W}^T d\mathbf{R}$. (Hence $d\hat{\phi}^{0,\mathcal{E}}$ and $d\hat{\mathbf{R}}^\mathcal{E}$ are vectors of length $n_\mathcal{E}$; and $d\hat{\phi}^{0,\mathcal{R}}$ and $d\hat{\mathbf{R}}^\mathcal{R}$ are vectors of length $n_\mathcal{R}$.) From

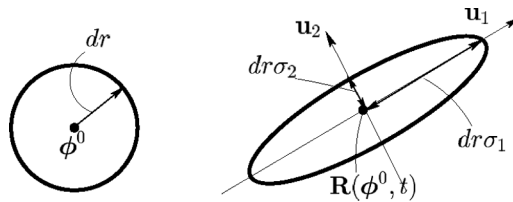


Figure 1. For a two-dimensional composition space, sketch showing the infinitesimal ball of radius dr at ϕ^0 mapped after time t to the infinitesimal ellipse at $\mathbf{R}(\phi^0, t)$. The principal semi-axes are $dr\sigma_1\mathbf{u}_1$ and $dr\sigma_2\mathbf{u}_2$, where σ_i and \mathbf{u}_i are the singular values and left singular vectors of the sensitivity matrix \mathbf{A} .

equations (22)–(24), we have

$$\begin{bmatrix} d\hat{\mathbf{R}}^\mathcal{E} \\ d\hat{\mathbf{R}}^\mathcal{R} \end{bmatrix} = \begin{bmatrix} \mathbf{I} & 0 \\ \frac{\partial \hat{\mathbf{R}}^\mathcal{R}}{\partial \hat{\phi}^{0,\mathcal{E}}} & \frac{\partial \hat{\mathbf{R}}^\mathcal{R}}{\partial \hat{\phi}^{0,\mathcal{R}}} \end{bmatrix} \begin{bmatrix} d\hat{\phi}^{0,\mathcal{E}} \\ d\hat{\phi}^{0,\mathcal{R}} \end{bmatrix} = \begin{bmatrix} \mathbf{I} & 0 \\ \mathbf{A}^{\mathcal{R},\mathcal{E}} & \mathbf{A}^{\mathcal{R},\mathcal{R}} \end{bmatrix} \begin{bmatrix} d\hat{\phi}^{0,\mathcal{E}} \\ d\hat{\phi}^{0,\mathcal{R}} \end{bmatrix}, \quad (25)$$

where $\mathbf{A}^{\mathcal{R},\mathcal{E}} = \frac{\partial \hat{\mathbf{R}}^\mathcal{R}}{\partial \hat{\phi}^{0,\mathcal{E}}}$ and $\mathbf{A}^{\mathcal{R},\mathcal{R}} = \frac{\partial \hat{\mathbf{R}}^\mathcal{R}}{\partial \hat{\phi}^{0,\mathcal{R}}}$. It is readily shown that $\mathbf{A}^{\mathcal{R},\mathcal{R}}$ is related to the sensitivity matrix \mathbf{A} by

$$\mathbf{A}^{\mathcal{R},\mathcal{R}} = \mathbf{W}^T \mathbf{A} \mathbf{W}. \quad (26)$$

At $t = 0$, $\mathbf{A}^{\mathcal{R},\mathcal{R}}$ is an $n_{\mathcal{R}} \times n_{\mathcal{R}}$ identity matrix.

At chemical equilibrium ($t \rightarrow \infty$), from equation (3) and (25), we have

$$\begin{aligned} d\mathbf{R}(\phi^0, \infty) &= d\mathbf{R}^\mathcal{E}(\phi^0, \infty) + d\mathbf{R}^\mathcal{R}(\phi^0, \infty) \\ &= \hat{\mathbf{C}} d\hat{\mathbf{R}}^\mathcal{E}(\phi^0, \infty) + \mathbf{W} d\hat{\mathbf{R}}^\mathcal{R}(\phi^0, \infty) \\ &= \hat{\mathbf{C}} d\hat{\phi}^{0,\mathcal{E}} + \mathbf{W}(\mathbf{A}^{\mathcal{R},\mathcal{E}} d\hat{\phi}^{0,\mathcal{E}} + \mathbf{A}^{\mathcal{R},\mathcal{R}} d\hat{\phi}^{0,\mathcal{R}}) \\ &= (\hat{\mathbf{C}} + \mathbf{W} \mathbf{A}^{\mathcal{R},\mathcal{E}}) d\hat{\phi}^{0,\mathcal{E}} + \mathbf{W} \mathbf{A}^{\mathcal{R},\mathcal{R}} d\hat{\phi}^{0,\mathcal{R}}. \end{aligned} \quad (27)$$

At chemical equilibrium, $\mathbf{R}(\phi^0, \infty)$ is independent of $\phi^{0,\mathcal{R}}$. This means that the term $\mathbf{W} \mathbf{A}^{\mathcal{R},\mathcal{R}} d\hat{\phi}^{0,\mathcal{R}}$ is zero for arbitrary $d\hat{\phi}^{0,\mathcal{R}}$. Therefore when the trajectory reaches chemical equilibrium, the singular values of matrix $\mathbf{A}^{\mathcal{R},\mathcal{R}}$ are zero, and the initial n_ϕ -dimensional hypersphere is mapped to an $n_\mathcal{E}$ dimensional hyper-ellipsoid.

3.2 Mapping of an infinitesimal ball in the reactive subspace

We can consider an initial infinitesimal ball centred at the initial point in the reactive subspace and take a geometrical view of the flow from this initial ball. (Note that the dimension of the ball is $n_{\mathcal{R}}$ and that all the trajectories starting from the points in the ball have the same chemical equilibrium composition.) From equation (25), we have

$$d\hat{\mathbf{R}}^\mathcal{R} = \mathbf{A}^{\mathcal{R},\mathcal{R}} d\hat{\phi}^{0,\mathcal{R}}, \quad (28)$$

for $d\hat{\phi}^{0,\mathcal{E}} = 0$.

Let the singular value decomposition (SVD) of $\mathbf{A}^{\mathcal{R},\mathcal{R}}$ be

$$\mathbf{A}^{\mathcal{R},\mathcal{R}} = \hat{\mathbf{U}} \hat{\Sigma} \hat{\mathbf{V}}^T, \quad (29)$$

where $\hat{\mathbf{U}}$ and $\hat{\mathbf{V}}$ are $n_{\mathcal{R}} \times n_{\mathcal{R}}$ orthogonal matrices and $\hat{\Sigma}$ is the diagonal matrix of singular values, $\hat{\sigma}_1 \geq \hat{\sigma}_2 \geq \dots \geq \hat{\sigma}_{n_{\mathcal{R}}} \geq 0$. The columns of $\hat{\mathbf{U}}$ ($\hat{\mathbf{u}}_i, i = 1, 2, \dots, n_{\mathcal{R}}$) and the columns of $\hat{\mathbf{V}}$ ($\hat{\mathbf{v}}_i, i = 1, 2, \dots, n_{\mathcal{R}}$) are the left and right singular vectors, respectively. Following the same procedure, it is readily shown that the infinitesimal ball in the reactive subspace centered at the initial composition ϕ^0

$$\{\phi = \phi^0 + \mathbf{W} d\hat{\phi}^{0,\mathcal{R}} \mid \|d\hat{\phi}^{0,\mathcal{R}}\| \leq dr\} \quad (30)$$

is mapped to the hyper-ellipsoid in the reactive subspace

$$\{\phi = \mathbf{R} + \mathbf{W} d\hat{\mathbf{R}}^\mathcal{R} \mid \|\mathbf{A}^{\mathcal{R},\mathcal{R}-1} d\hat{\mathbf{R}}^\mathcal{R}\| \leq dr\}, \quad (31)$$

or, equivalently,

$$\{\phi = \mathbf{R} + \mathbf{W}d\hat{\mathbf{R}}^{\mathcal{R}} \mid \|\hat{\Sigma}^{-1}\hat{\mathbf{U}}^T d\hat{\mathbf{R}}^{\mathcal{R}}\| \leq dr\}, \quad (32)$$

which is centred at the reaction mapping $\mathbf{R}(\phi^0, t)$. The principal semi-axes of the hyperellipsoid are $dr\hat{\sigma}_i\hat{\mathbf{u}}_i$, $i = 1, 2, \dots, n_{\mathcal{R}}$, where $\hat{\mathbf{u}}_i$ is the i th column of $\hat{\mathbf{U}}$. Notice that at the equilibrium point, the initial $n_{\mathcal{R}}$ -dimensional ball is mapped to a single point. So, along the trajectory, the dimension of the object decreases from $n_{\mathcal{R}}$ initially to zero in infinite time.

3.3 Mapping of the rate vector

Besides the above geometrical significance, the sensitivity matrix also provides a link between the rate vector at $\mathbf{R}(\phi^0, t)$ and the rate vector at the initial point ϕ^0 . If the time along the trajectory is increased from t to $t + dt$, the final composition is

$$\mathbf{R}(\phi^0, t + dt) = \mathbf{R}(\phi^0, t) + \mathbf{S}(\mathbf{R}(\phi^0, t)) dt. \quad (33)$$

The same composition results if the initial condition, instead of being ϕ^0 , is taken to be $\mathbf{R}(\phi^0, dt) = \phi^0 + \mathbf{S}(\phi^0) dt$, i.e.

$$\mathbf{R}(\phi^0, t + dt) = \mathbf{R}(\phi^0 + \mathbf{S}(\phi^0) dt, t). \quad (34)$$

From equations (18), (33) and (34) we have

$$\mathbf{S}(\mathbf{R}(\phi^0, t)) = \mathbf{A}\mathbf{S}(\phi^0). \quad (35)$$

Thus the rate vector at $\mathbf{R}(\phi^0, t)$ is related to the rate vector at ϕ^0 through the sensitivity matrix.

4. Results

In this work, we study reaction trajectories starting from a wide range of different initial composition for both H_2/air and CH_4/air systems. The initial compositions we consider are either: randomly chosen from the composition space; or from the compositions resulting from the autoignition of pure fuel/air mixtures; or from the mixing line between the pure fuel/air mixture and its corresponding equilibrium point in the composition space; or from the composition in one-dimensional laminar flames computed by SANDIA's PREMIX and OPPDIF codes. Table 1 lists some of the initial compositions. The pressure is atmospheric for all cases studied in this paper. For the results presented below, comprehensive tests were performed in order to ensure numerical accuracy.

Table 1. Test cases and the methods of generating initial compositions.

H ₂ -1	Autoignition of a stoichiometric H ₂ /air mixture at the initial temperature 300 K
H ₂ -2	Autoignition of a stoichiometric H ₂ /air mixture at the initial temperature 1000 K
H ₂ -3	Unstrained, one-dimensional, laminar premixed flame of stoichiometric H ₂ /air at 300 K
CH ₄ -1	Autoignition of a stoichiometric CH ₄ /air mixture at the initial temperature 300 K
CH ₄ -2	Autoignition of a stoichiometric CH ₄ /air mixture at the initial temperature 1500 K
CH ₄ -3	Unstrained, one-dimensional, laminar premixed flame of stoichiometric CH ₄ /air at 300 K

For H_2/air combustion, the Mueller mechanism [25], which has 9 species and 21 reactions, is employed. Hence the dimension for the full composition space is 10 and the dimension of the reactive subspace is 6. This mechanism has been updated by Li *et al.* [26]; however, the differences are unlikely to affect any of the conclusions drawn.

For CH_4/air combustion, the GRI3.0 mechanisms [27] with and without nitrogen chemistry are employed. The GRI3.0 mechanism without nitrogen chemistry is generated from the standard GRI3.0 mechanism by stripping out all the N-containing species and reactions except for N_2 . The GRI3.0 mechanisms with and without nitrogen chemistry have 53 and 36 species, respectively, and therefore the dimensions of the full composition spaces are 54 and 37, and the dimensions of the reactive subspaces are 48 and 31.

4.1 Dimensionality of reaction trajectories

To address questions concerning the accessed compositions in reactive flows, an important issue is to determine the dimensionality of the affine space (denoted by n'_R) containing individual reaction trajectories, i.e. the dimensionality of the tangent bundle along a trajectory [15]. If the trajectory is a line segment (and hence has no curvature) then $n'_R = 1$. In general we have $1 \leq n'_R \leq n_R$. Here the dimensionality of the tangent bundle for different trajectories and mechanisms is determined.

As illustrated in figure 2, the trajectory is parameterized by arclength, s , with $\phi(s=0) = \phi^0$ and $\phi(s=s_{eq}) = \phi^{eq}$, where s_{eq} is the total arclength of the trajectory and ϕ^{eq} is the equilibrium point. Proceeding backwards from the equilibrium point, the trajectory is decomposed into N segments, each having the same arclength $\Delta s = s_{eq}/N$. The composition increment $\Delta\phi^i$ ($i = 1, 2, \dots, N$) is defined as the difference between the corresponding beginning and ending compositions. As N approaches infinity (i.e. Δs approaches 0), the unit tangent vector for each segment of the trajectory is well approximated by $\mathbf{T}^i = \frac{\Delta\phi^i}{\|\Delta\phi^i\|}$, and the curvature along the trajectory is well approximated by $\kappa(s = i \times \Delta s) = \|\mathbf{T}^{i+1} - \mathbf{T}^i\|/\Delta s$, where $i = 1, 2, \dots, N$.

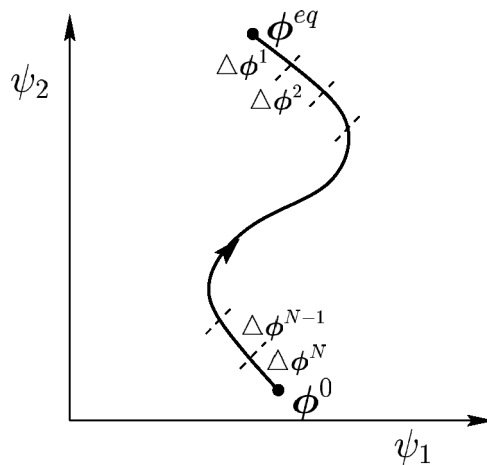


Figure 2. Trajectory in composition space: ϕ^0 and ϕ^{eq} denote the initial composition and the corresponding equilibrium composition. Proceeding backwards from the equilibrium point, the trajectory is decomposed into N segments, each having the same arclength Δs . Symbol $\Delta\phi^i$ denotes the composition difference between the corresponding beginning and ending compositions.

For fixed N , proceeding backwards from the equilibrium point, we form the following matrices containing the unit tangent vectors (or tangent bundle matrices)

$$\begin{aligned} \bar{\mathbf{T}}_1 &= [\mathbf{T}^1] \\ &\vdots \\ \bar{\mathbf{T}}_k &= \frac{1}{\sqrt{k}}[\mathbf{T}^1 \quad \mathbf{T}^2 \dots \mathbf{T}^k] \\ &\vdots \\ \bar{\mathbf{T}}_N &= \frac{1}{\sqrt{N}}[\mathbf{T}^1 \quad \mathbf{T}^2 \dots \mathbf{T}^N]. \end{aligned} \quad (36)$$

The normalization factor $1/\sqrt{k}$ is chosen so that all the singular values of the above tangent bundle matrices are between 0 and 1, and the results shown below becomes independent of the parameter N , as N approaches infinity. The k columns of the matrix $\bar{\mathbf{T}}_k$ are proportional to the tangent vectors over the final k segments of the reaction trajectory, and hence they span the tangent bundle of this part of the trajectory. The dimensionality of the tangent bundle is, therefore, the rank of $\bar{\mathbf{T}}_k$, which can be determined through the singular values of the matrix: small (less than some threshold value, i.e. $\bar{\sigma}_i < \epsilon$) or zero singular values indicate rank deficiency. As the distance from the equilibrium point increases, the dimensionality of the affine space increases.

Figure 3 shows the singular values of the tangent bundle matrices and the dimensionality of the affine space containing the trajectory proceeding backwards from the equilibrium point for H_2/air mixtures along one trajectory in the composition space, using different values of the numerical parameters N and threshold ϵ . As may be seen from figure 3, there is no noticeable difference in the numerically computed singular values of the tangent bundle matrices between $N = 800$ and $N = 1200$. Therefore the results for the singular values of the tangent bundle matrices are numerically accurate. Also figure 3 shows the effect of the threshold ϵ . As expected, for a smaller value of the threshold ϵ , proceeding backwards from the equilibrium point, the dimension of the affine space increases earlier. However for a wide range of trajectories, the dimensionality of the affine space is found to be insensitive to the value of threshold ϵ . The results reported below (figures 4–6) are obtained with $N = 1200$ and $\epsilon = 0.01$.

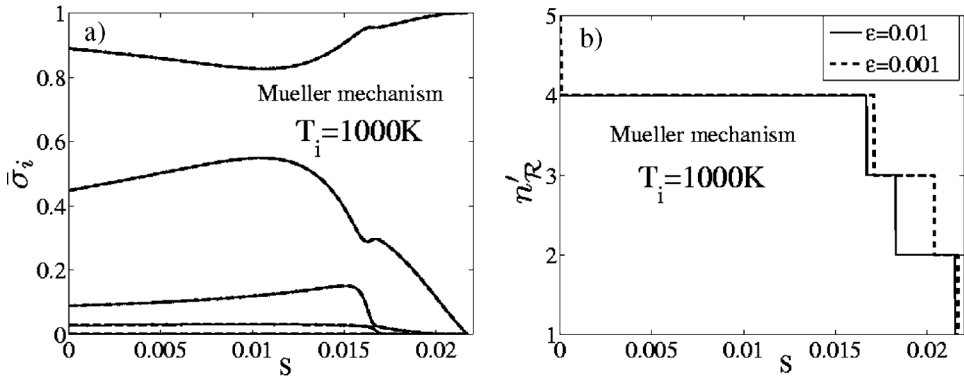


Figure 3. (a) Singular values of the tangent bundle matrices proceeding backwards from the equilibrium points; dash line: $N = 800$; solid line: $N = 1200$. (b) The dimensionality of the affine space containing the trajectory proceeding backwards from the equilibrium points with two threshold different ϵ values and $N = 1200$. The trajectory starts from the initial composition $\text{H}_2 - 2$ in table 1 with temperature 1000 K.

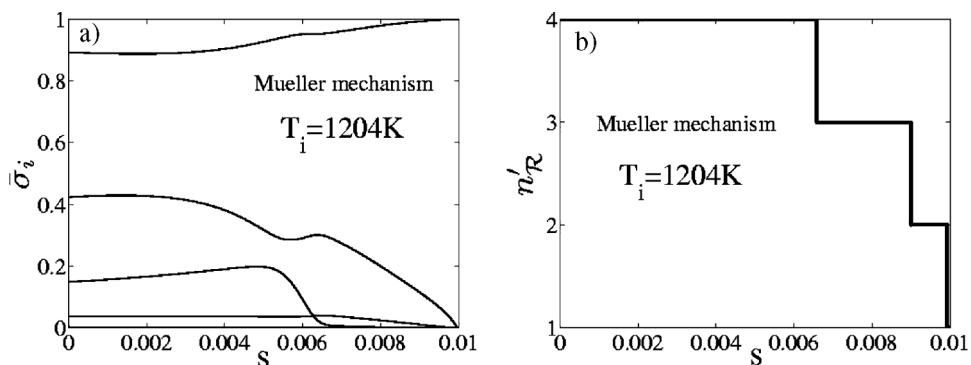


Figure 4. (a) Singular values of the tangent bundle matrices proceeding backwards from the equilibrium points. (b) The dimensionality of the affine space containing the trajectory proceeding backwards from the equilibrium points. The trajectory starts from the initial composition $H_2 - 3$ in table 1 with temperature 1204 K. The threshold ϵ is 0.01 and $N = 1200$.

As may be seen from figures 3 and 4, for the H_2 /air mixtures, proceeding backwards from the equilibrium points, the dimensionality of the affine space increase from 1 to 4 for these two cases. (For H_2 /air with the Mueller mechanism, the dimensionality of the reactive subspace is 6.) The singular value in one direction is much larger than all other singular values, which implies that the trajectory is aligned with that direction.

Figure 5 shows the results for CH_4 /air mixtures along two representative trajectories. Proceeding backwards from the equilibrium point, the dimensionality of the affine space increases, but it remains much smaller than the dimension of the full composition space. For CH_4 /air, the maximum dimension observed is $n'_R = 11$, whereas the dimensions of the reactive subspaces are 48 and 31 for GRI3.0 with and without nitrogen chemistry. Nitrogen chemistry increases the dimension of the affine space as expected. However, the number of dimensions increased

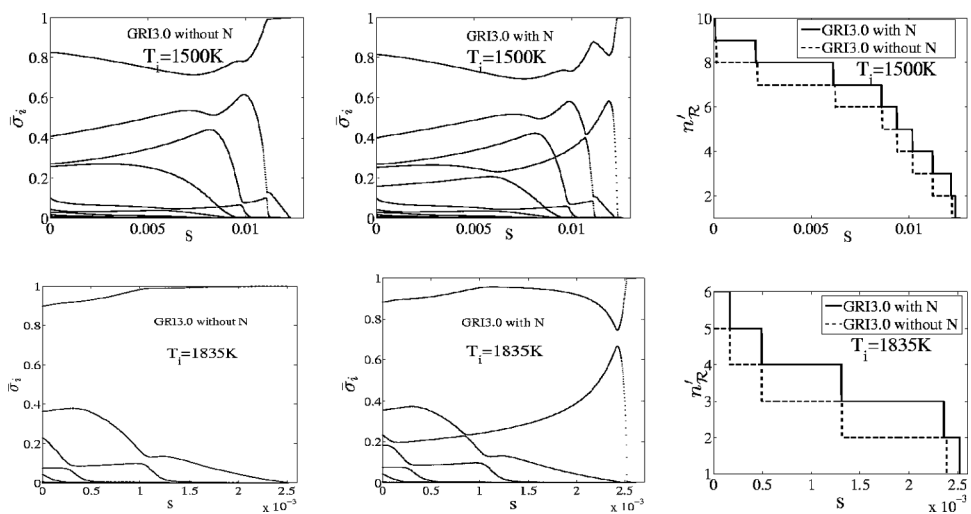


Figure 5. First and second columns: singular values of the tangent bundle matrices proceeding backwards from the equilibrium points; third column: the dimensionality of the affine space containing the trajectory proceeding backwards from the equilibrium points. First row: the trajectory starts from the initial composition $CH_4 - 2$ in table 1 with temperature 1500 K; second row: $CH_4 - 3$ with temperature 1835 K. The threshold ϵ is 0.01 and $N = 1200$.

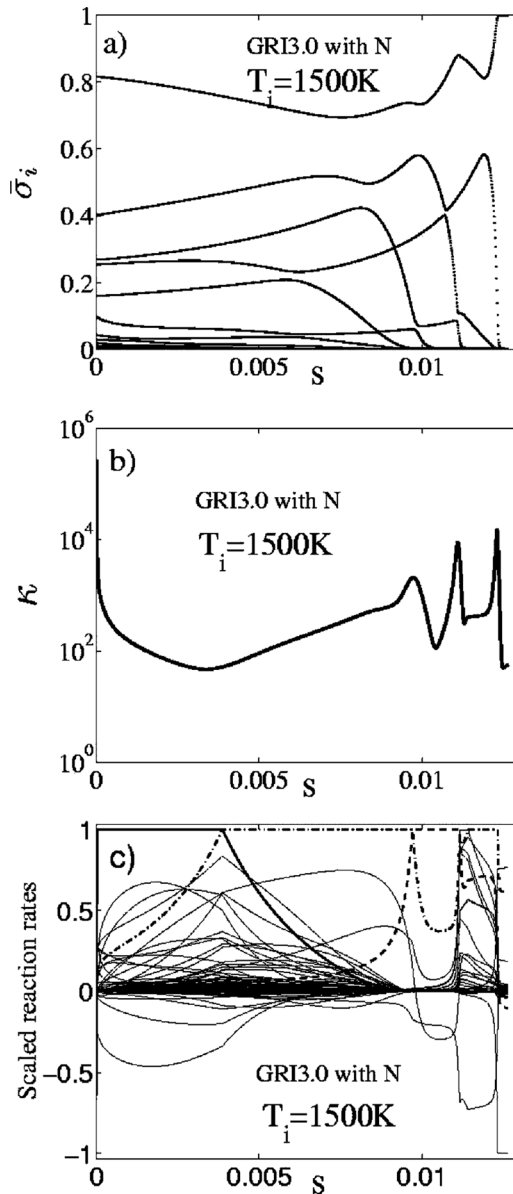


Figure 6. (a) Singular values of the tangent bundle matrices proceeding backwards from the equilibrium point; (b) the curvature κ (unit: $(\text{kmol/kg})^{-1}$) along the trajectory; (c) normalized reaction rate of the elementary reactions (normalized by the maximum elementary reaction rate in magnitude) along the trajectory. The trajectory start from the initial composition $\text{CH}_4 - 2$ in table 1 with temperature 1500 K.

(about 1 and 2 for these two cases) is much smaller than the number of the dimensions added to the system (17) by the nitrogen chemistry. This is because all of the nitrogen species have relatively small concentrations (except N_2) and nitrogen chemistry is active only at high temperatures (close to equilibrium). The difference in the singular values of the tangent bundle matrices close to equilibrium for the same case between GRI3.0 with and without nitrogen chemistry is also due to the fact that nitrogen chemistry is active and the trajectory close to equilibrium (at high temperatures) is mostly determined by the nitrogen chemistry.

The dimensionality of the affine space is highly related to the curvature along the trajectory. If the trajectory has no curvature (i.e. it is a line segment), the dimensionality of the affine space is 1. Figure 6 shows the singular values of the tangent bundle matrices, the curvature and the normalized reaction rate of the elementary reactions (normalized by the maximum elementary reaction rate in magnitude) along the trajectory. As may be seen from the figure, proceeding backwards from the equilibrium point, new nontrivial singular values (greater than some threshold ϵ) arise where the curvature is large. Also from the figure, we observe that large curvature occurs where the reaction path changes, i.e. the dominant reactions change along the trajectory.

4.2 Spectra of eigenvalues of the Jacobian matrices

An important quantity in studying the time-scales and stability of a set of differential equations is the Jacobian. For a chemical system, the eigenvalues of the Jacobian matrix of the reaction source term are related to the chemical time scales with $\tau_i = 1/|\lambda_i^r|$, where λ_i^r denotes the real part of the i th eigenvalue. Moreover, there are $n_e + 1$ eigenvalues which are exactly zeros due to the conservation of elements and enthalpy in the reaction process. Also the Jacobian matrix contains the information which describes the short-time evolution of a small perturbation to the nonlinear chemical system [6, 14, 28]. For $\lambda_i^r > 0$, the magnitude of the perturbation increases; for $\lambda_i^r = 0$, the magnitude of the perturbation does not change with time; for $\lambda_i^r < 0$, the magnitude of the perturbation relaxes to zero. A Jacobian matrix with a set of eigenvalues with large negative real parts implies the existence of a low-dimensional attracting manifold in the composition space.

It is informative to look at some representative spectra of the eigenvalues of the Jacobian, which provide the characteristic chemical times scales. Figures 7, 9 and 10 show three representative spectra of eigenvalues along trajectories for both H_2/air and CH_4/air mixtures. The figures show the real parts of the eigenvalues which are either greater than 1 s^{-1} or less than -1 s^{-1} along the trajectories parameterized by temperature. In figure 7, trajectories start from pure stoichiometric H_2/air mixture and pure stoichiometric CH_4/air mixture at the low initial temperature 300 K. As may be seen from figure 7, there are many large (in magnitude) negative eigenvalues for both CH_4/air and H_2/air mixtures even at low temperatures. (Figure 8 characterizes eigenvalues of CH_4/air mixture at temperature 300 K. As may be seen from figure 8, for the GRI3.0 mechanism with nitrogen chemistry, there are 13 eigenvalues whose real parts are smaller than $-1 \times 10^5 \text{ s}^{-1}$.) With the increase of temperature along the trajectories, the number of small eigenvalues increases. Positive eigenvalues and conjugate eigenvalue pairs are observed for both CH_4/air and H_2/air mixtures. For the H_2/air mixture, between around 900 K and 1300 K, there are positive eigenvalues and a conjugate eigenvalue pair. For the CH_4/air mixture, between around 800 K and 1700 K, there is a positive eigenvalue; around 1700 K, there is a conjugate eigenvalue pair. Also in figure 7, it may be observed that the ordering of eigenvalues changes along the trajectories.

Based on the spectra of eigenvalues, we see that the hydrogen mechanism plays a very important role in the methane combustion: the structure of the spectrum of eigenvalues for the hydrogen mechanism can be observed in the spectrum of eigenvalues for the methane combustion. For methane combustion using the GRI3.0 mechanism with or without nitrogen chemistry, we notice that nitrogen chemistry adds a relative large eigenvalue (corresponding to the slow process in nitrogen chemistry).

Figure 9 shows the same case but with a higher initial temperature. Similar phenomena are also observed for the high-temperature region. The trajectories in figure 10 start from compositions obtained from one-dimensional laminar premixed flames for pure stoichiometric

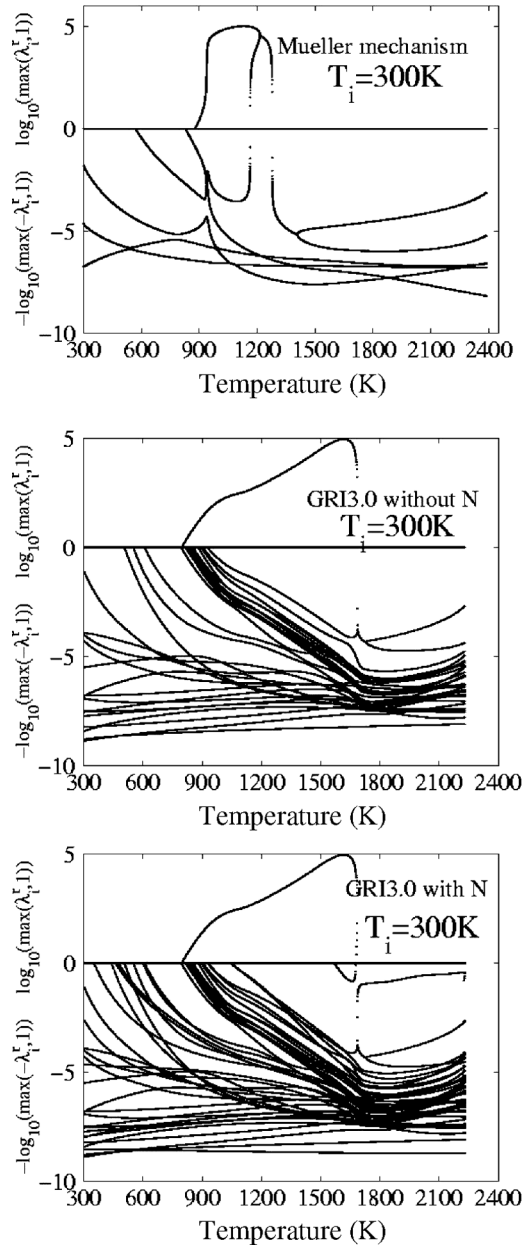


Figure 7. Real parts of eigenvalues (unit: s^{-1}) of the Jacobian against temperature along the trajectories starting from the initial compositions $H_2 - 1$ and $CH_4 - 1$ in table 1, respectively.

fuel/air mixtures with unburnt temperatures of 300 K. As may be seen from figure 10, for this case, all the real parts of the eigenvalues (except the $n_e + 1$ zero eigenvalues) are negative.

By studying the eigenvalue spectra along trajectories, even at low temperatures, a wide range of time scales in the chemical system is observed. Therefore it is reasonable to assume the existence of low-dimensional attracting manifolds in the composition space. For a given

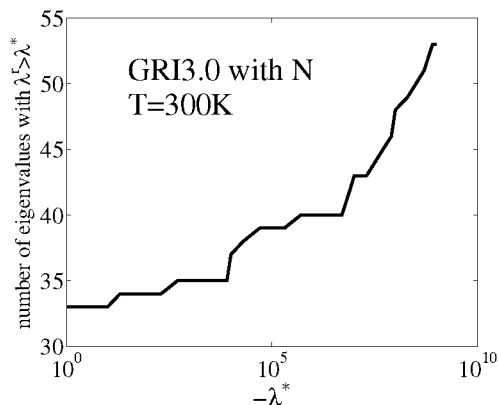


Figure 8. Real parts of eigenvalues (unit: s^{-1}) of the Jacobian for stoichiometric CH_4/air mixture at temperature 300 K.

chemical system, the questions needing to be addressed are: what is the required dimension of the attracting manifold to describe the particular system? How can the low-dimensional attracting manifold be identified? In the following sections, based on the sensitivity matrices, a new method is proposed to determine the minimum dimension of the attracting manifolds required for describing a chemical system with prescribed accuracy and to identify the ‘principal subspace’ which is an approximation to the tangent space of the attracting manifold.

4.3 Spectra of singular values of the sensitivity matrices

The geometrical significance of the sensitivity matrix is explained in section 3. The sensitivity matrix provides information about the behaviour of the flow from the vicinity of the initial point of the trajectory considered. Along this trajectory, at different times, the initial infinitesimal ball in the reactive subspace centred at the initial point is mapped to a hyper-ellipsoid, and at infinite time it contracts to a point, which is the corresponding equilibrium point. Moreover the singular value decomposition of the sensitivity matrix characterizes the geometry of the hyper-ellipsoid along the trajectory. Therefore it is worthwhile to study some representative spectra of the singular values (in the reactive subspace) along trajectories.

Figure 11 shows the spectra of singular values along the trajectories for H_2/air and CH_4/air autoignition. In this case the trajectories start from pure stoichiometric H_2/air with initial temperature 1000 K, and from the pure CH_4/air with initial temperature 1500 K, respectively. As may be seen from the figure, for both H_2/air and CH_4/air mixtures, most singular values decrease from one towards zero quickly, well before reaching equilibrium. Gradually, all the singular values decrease towards zero at the equilibrium point. The large singular value is due to presence of positive eigenvalues (see figure 9) in this particular case. This corresponds to accelerating reaction along the trajectory. For the CH_4/air autoignition, the sharp transition around 2350 K where many singular values drop rapidly is due to the sharp transition in the spectra of eigenvalues (see figure 9) where the positive eigenvalues become negative. Also we observe that nitrogen chemistry adds one relatively large and slowly decreasing singular value, which corresponds to the slow process in the nitrogen chemistry.

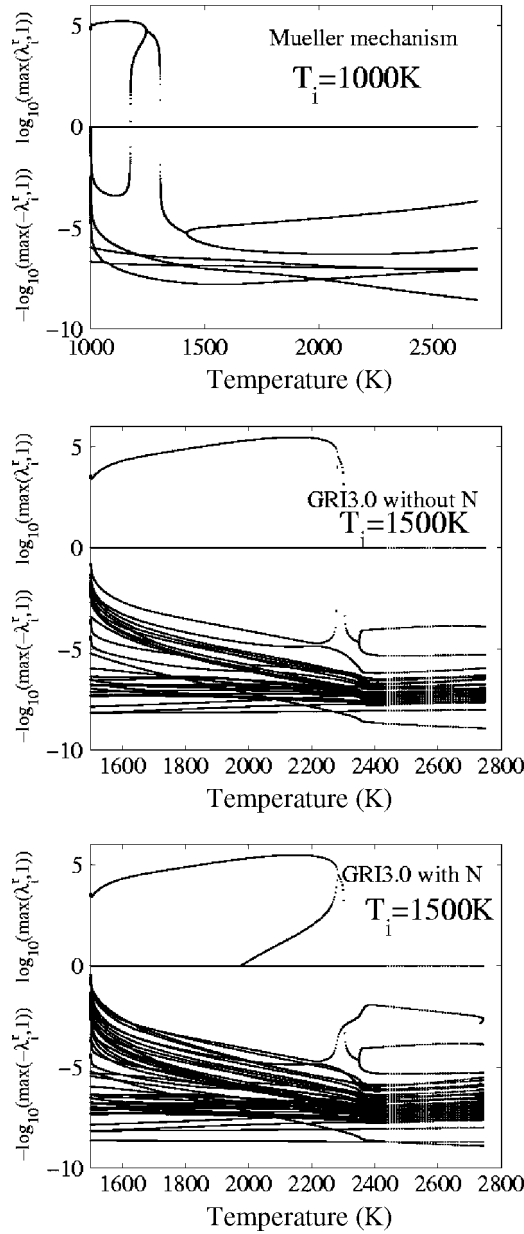


Figure 9. Real parts of eigenvalues (unit: s^{-1}) of the Jacobian against temperature along the trajectories starting from the initial compositions $H_2 - 2$ and $CH_4 - 2$ in table 1, respectively.

Figure 12 shows another spectrum of singular values. In this case, the trajectories start from the compositions obtained from one-dimensional premixed laminar flames of pure stoichiometric fuel/air mixtures with unburnt temperatures of 300 K. The same observations apply except that for this case there is no positive eigenvalues (see figure 10) so there is no large singular value compared with the previous case, although several are greater than unity at early times. Nor is there the sharp transition for CH_4 /air observed in figure 11.

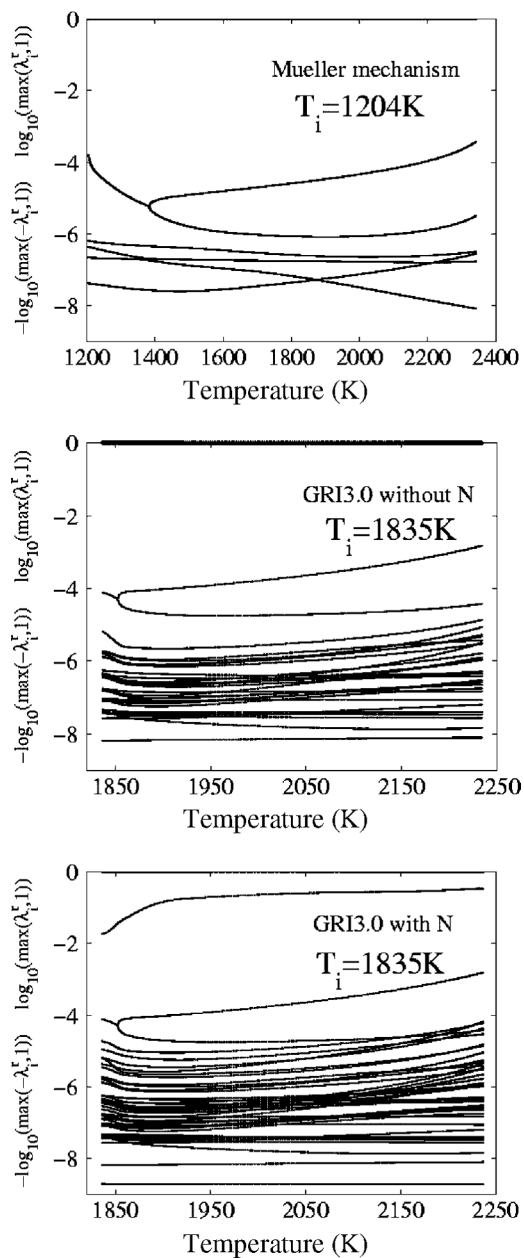


Figure 10. Real parts of eigenvalues (unit: s^{-1}) of the Jacobian against temperature along the trajectories starting from the initial compositions $H_2 - 3$ and $CH_4 - 3$ in table 1, respectively.

4.4 Attracting manifolds

As a result of the wide range of time scales in the chemical system, after the initial transient, the sensitivity matrix has a wide range of singular values. Along the trajectory, most singular values decrease from one towards zero very quickly, well before reaching the equilibrium point (see figures 11 and 12). This implies an effective dimension decrease of the initial ball

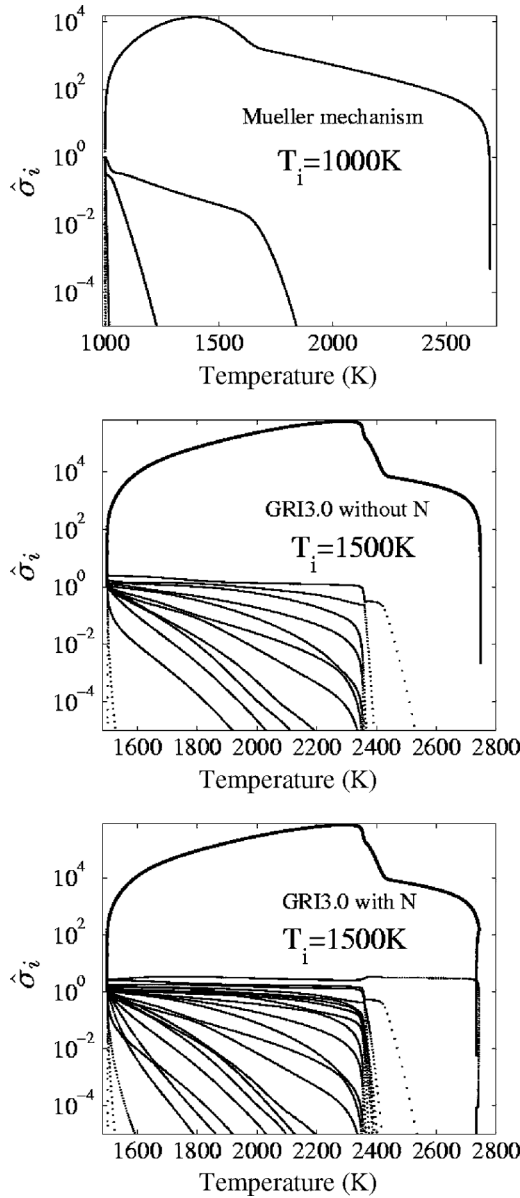


Figure 11. Singular values of the sensitivity matrices $\mathbf{A}^{\mathcal{R}, \mathcal{R}}$ against temperature along the trajectories starting from the initial compositions $\text{H}_2 - 2$ and $\text{CH}_4 - 2$ in table 1, respectively.

along the trajectory. Geometrically, in the reactive subspace, after the initial transient, the initial ball becomes a hyper-ellipsoid and is attracted to and aligned with a low-dimensional attracting manifold.

Based on these considerations we define the dimension of the attracting manifold as follows. Given a small positive threshold ϵ ($0 < \epsilon \ll 1$), the dimension $d_\epsilon(t)$ of the attracting manifold after a time t along the reaction trajectory from the given initial condition ϕ^0 , is defined to be the number of singular values $\hat{\sigma}_i(\phi^0, t)$ that are greater than ϵ . Recall that $\hat{\sigma}_i(\phi^0, t)$ denotes

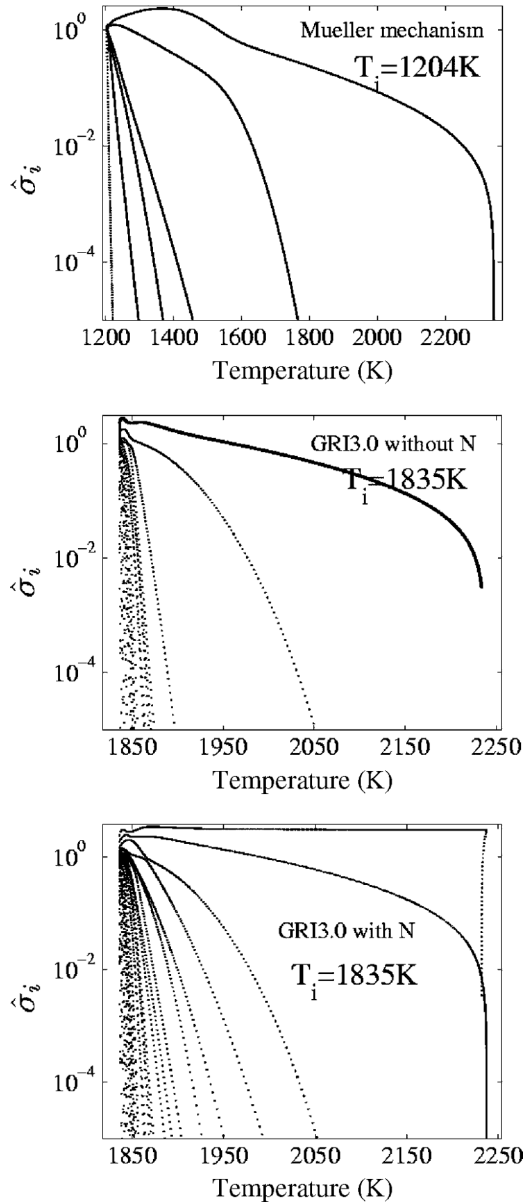


Figure 12. Singular values of the sensitivity matrices $\mathbf{A}^{\mathcal{R},\mathcal{R}}$ against temperature along the trajectories starting from the initial compositions $\text{H}_2 - 3$ and $\text{CH}_4 - 3$ in table 1, respectively.

the i th singular value of $\mathbf{A}^{\mathcal{R},\mathcal{R}}$ which is defined in equation (25) and related to \mathbf{A} by equation (26).

At the initial point, $\mathbf{A}^{\mathcal{R},\mathcal{R}}$ is the $n_{\mathcal{R}} \times n_{\mathcal{R}}$ identity matrix and has $n_{\mathcal{R}}$ singular values of unity, so $d_{\epsilon}(t=0) = n_{\mathcal{R}}$. At the equilibrium point, all the singular values of $\mathbf{A}^{\mathcal{R},\mathcal{R}}$ are zero, so $d_{\epsilon}(t=\infty) = 0$ as expected.

With ϵ specified, we consider an intermediate time t such that $n_{\mathcal{R}} > d_{\epsilon}(t) > 0$. Considering the initial infinitesimal perturbation in the reactive subspace ($d\hat{\phi}^{0,\epsilon} = 0$), from equations (28)

and (29), we have

$$\begin{aligned}
d\mathbf{R}^{\mathcal{R}} &= \mathbf{W}d\hat{\mathbf{R}}^{\mathcal{R}} = \mathbf{W}\mathbf{A}^{\mathcal{R},\mathcal{R}}d\hat{\phi}^{0,\mathcal{R}} \\
&= \mathbf{W}\hat{\mathbf{U}}\hat{\Sigma}\hat{\mathbf{V}}^T d\hat{\phi}^{0,\mathcal{R}} = \tilde{\mathbf{U}}\tilde{\Sigma}\tilde{\mathbf{V}}^T d\hat{\phi}^{0,\mathcal{R}} \\
&= [\mathbf{U}^> \ \mathbf{U}^<] \begin{bmatrix} \Sigma^> & 0 \\ 0 & \Sigma^< \end{bmatrix} [\mathbf{V}^> \ \mathbf{V}^<]^T d\hat{\phi}^{0,\mathcal{R}} \\
&= \mathbf{U}^>\Sigma^>\mathbf{V}^>^T d\hat{\phi}^{0,\mathcal{R}} + \mathbf{U}^<\Sigma^<\mathbf{V}^<^T d\hat{\phi}^{0,\mathcal{R}}, \tag{37}
\end{aligned}$$

where $\tilde{\mathbf{U}} = \mathbf{W}\hat{\mathbf{U}}$ and its orthonormal columns span the reactive subspace \mathcal{R} , $\Sigma^>$ is a $d_\epsilon \times d_\epsilon$ diagonal matrix with $\sigma_i^> > \epsilon$, and $\Sigma^<$ is a $(n_{\mathcal{R}} - d_\epsilon) \times (n_{\mathcal{R}} - d_\epsilon)$ diagonal matrix with $\sigma_i^< \leq \epsilon$. The matrices $\mathbf{U}^>$ and $\mathbf{U}^<$ are $n_\phi \times d_\epsilon$ and $n_\phi \times (n_{\mathcal{R}} - d_\epsilon)$ matrices, respectively; $\mathbf{V}^>$ and $\mathbf{V}^<$ are $n_{\mathcal{R}} \times d_\epsilon$ and $n_{\mathcal{R}} \times (n_{\mathcal{R}} - d_\epsilon)$ matrices, respectively. Thus in the approximation that the singular values less than or equal to ϵ are negligible, we have

$$\begin{aligned}
d\mathbf{R}^{\mathcal{R}} &= \mathbf{U}^>\Sigma^>\mathbf{V}^>^T d\hat{\phi}^{0,\mathcal{R}} + d\mathbf{R}^\epsilon \\
&\approx \mathbf{U}^>\Sigma^>\mathbf{V}^>^T d\hat{\phi}^{0,\mathcal{R}}, \tag{38}
\end{aligned}$$

where the error $d\mathbf{R}^\epsilon$ satisfies

$$\begin{aligned}
\|d\mathbf{R}^\epsilon\| &= \|\mathbf{U}^<\Sigma^<\mathbf{V}^<^T d\hat{\phi}^{0,\mathcal{R}}\| \\
&\leq \epsilon \|d\hat{\phi}^{0,\mathcal{R}}\| = \epsilon \|d\hat{\phi}^{0,\mathcal{R}}\|. \tag{39}
\end{aligned}$$

So, as illustrated in figure 13, the infinitesimal $n_{\mathcal{R}}$ -dimensional ball of radius dr centred at ϕ^0 in the reactive subspace is mapped to within a distance of ϵdr of the d_ϵ -dimensional affine space which intersects $\mathbf{R}(\phi^0, t)$ and has tangent space $\text{span}(\mathbf{U}^>)$. Thus, in the reactive subspace, along the trajectory, the initial ball becomes a hyper-ellipsoid and is attracted to and aligned with a $d_\epsilon(t)$ -dimensional attracting manifold. The columns of $\mathbf{U}^>$ span the $d_\epsilon(t)$ -dimensional ‘principal subspace’ which is a good approximation to the tangent space of the $d_\epsilon(t)$ -dimensional attracting manifold; and the columns of $\mathbf{U}^<$ span the $(n_{\mathcal{R}} - d)$ -dimensional ‘compressive subspace’.

From equation (35), the reaction rate vector along the trajectory is related to the sensitivity matrix by

$$\mathbf{S}(\mathbf{R}(\phi^0, t)) = \mathbf{A}\mathbf{S}(\phi^0). \tag{40}$$

Because the rate vector has no components in the conserved subspace, equation (40) can also be written as

$$\begin{aligned}
\mathbf{S}(\mathbf{R}(\phi^0, t)) &= \mathbf{A}\mathbf{W}\mathbf{W}^T\mathbf{S}(\phi^0) = \mathbf{W}\mathbf{A}^{\mathcal{R},\mathcal{R}}\mathbf{W}^T\mathbf{S}(\phi^0) \\
&= [\mathbf{U}^> \ \mathbf{U}^<] \begin{bmatrix} \Sigma^> & 0 \\ 0 & \Sigma^< \end{bmatrix} [\mathbf{V}^> \ \mathbf{V}^<]^T \mathbf{W}^T\mathbf{S}(\phi^0) \\
&= \mathbf{U}^>\Sigma^>\mathbf{V}^>^T \mathbf{W}^T\mathbf{S}(\phi^0) + \mathbf{S}^\epsilon \\
&\approx \mathbf{U}^>\Sigma^>\mathbf{V}^>^T \mathbf{W}^T\mathbf{S}(\phi^0), \tag{41}
\end{aligned}$$

where the second step follows from equation (26) and the last step follows from the assumption that the singular values less than ϵ are neglected. The error \mathbf{S}^ϵ satisfies

$$\|\mathbf{S}^\epsilon\| \leq \epsilon \|\mathbf{S}(\phi^0)\|. \tag{42}$$

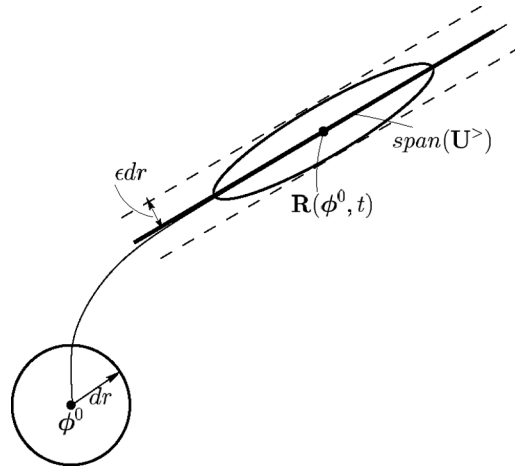


Figure 13. In the reactive subspace \mathcal{R} , the infinitesimal $n_{\mathcal{R}}$ -dimensional hypersphere of radius dr is mapped to within a distance ϵdr of the d_e -dimensional affine space (shown as the solid line). The affine space intersect $\mathbf{R}(\phi^0, t)$ and its tangent space is the principal subspace, $\text{span}(\mathbf{U}^>)$.

Equation (41) implies that, after the initial transient, the rate vector along the trajectory is in the $d_e(t)$ -dimensional ‘principal subspace’.

Figure 14 shows the reaction trajectories from different initial compositions for the H_2/air system. The initial compositions are randomly chosen from the composition space and have the same amount of elements and enthalpy. Therefore all the trajectories have the same chemical equilibrium. As may be seen from the figure, all the trajectories are attracted to a one-dimensional attracting manifold well before reaching chemical equilibrium. Based on the singular values of matrix $\mathbf{A}^{\mathcal{R},\mathcal{R}}$, the dimension of the attracting manifold along the reaction trajectory from each initial condition ϕ^0 is determined using threshold value $\epsilon = 0.001$. Geometrically, this implies that once the length of a principal axis of the hyper-ellipsoid reaches one-thousandth of the initial ball radius, the dimension associated with that direction

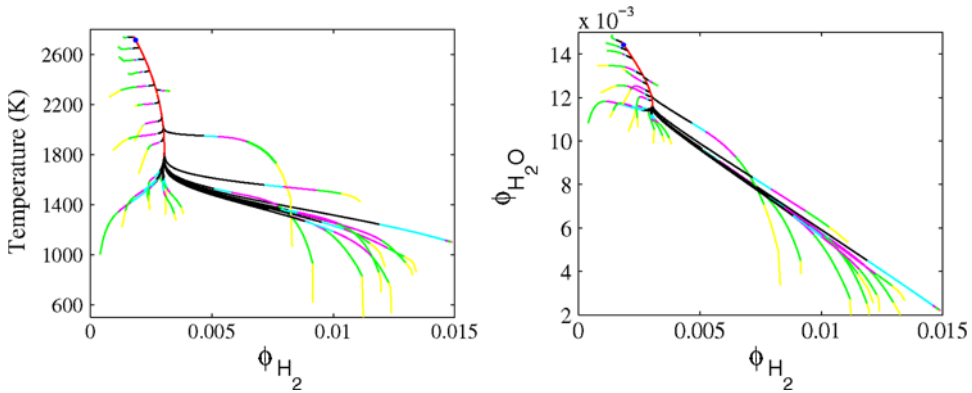


Figure 14. Projection onto different planes of the reaction trajectories for the H_2/air system with the Mueller mechanism. The initial compositions are chosen randomly from the composition space and have the same amount of elements and enthalpy (H: 0.03420 kmol/kg; O: 0.01697 kmol/kg; N: 0.04955 kmol/kg; enthalpy: 6.9021×10^9 k-ergs/kg). Each trajectory is coloured by the dimension of the attracting manifold determined based on the matrix $\mathbf{A}^{\mathcal{R},\mathcal{R}}$. Yellow: 6—dimensional; green: 5-dimensional; magenta: 4-dimensional; cyan: 3-dimensional; black: 2-dimensional; red: 1-dimensional; blue: 0-dimensional. The blue dot is the equilibrium point. The threshold ϵ is 0.001.

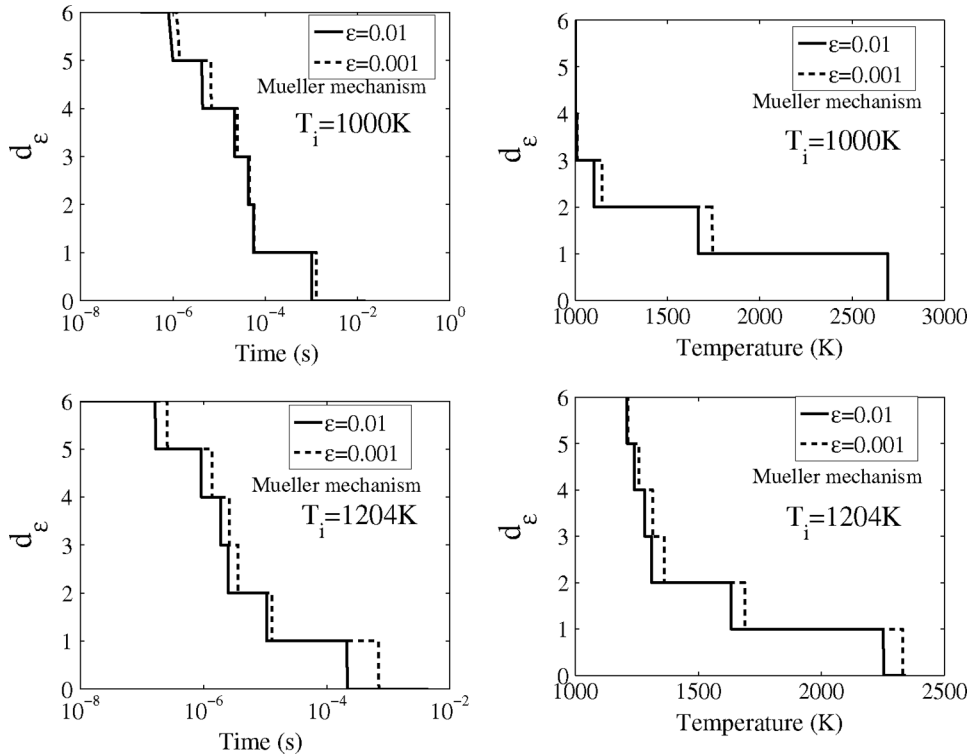


Figure 15. Dimension of the attracting manifold for H_2/air against time and temperature along the trajectories starting from different initial compositions. For the first row, the initial composition is chosen from $\text{H}_2 - 2$ in table 1. For the second row, the initial composition is chosen from $\text{H}_2 - 3$.

is neglected. In figure 14, each trajectory is coloured by the value of dimension. And along each trajectory the dimension of the attracting manifold decreases from 6 (coloured yellow) to zero (coloured blue) at equilibrium as expected. (For H_2/air autoignition with the Mueller mechanism, the dimension of the reactive subspace is 6.)

Figure 15 shows the dimension of the attracting manifold for the H_2/air mixture against time and temperature along the trajectories. In figure 15 we use two different thresholds, $\epsilon = 0.01$ and 0.001 , and as may be seen the difference between these two threshold values is not significant. As may be seen from figure 15, the dimension of the attracting manifold decreases from 6 to zero at equilibrium. After the initial transient, the dimension of the attracting manifold is much smaller than the dimension of the full composition space. With increasing initial temperature, the time for the initial transient to reach a given dimension of attracting manifold decreases. For the first row in figure 15 where the trajectory starts from a stoichiometric H_2/air mixture with initial temperature 1000 K, the time required to reach a three dimensional attracting manifold is about 2×10^{-5} s. However, with respect to the temperature, the initial transient is very quick (less than 1 K). For the last row in figure 15 where the trajectory starts from laminar flame results, the time required to reach a three dimensional attracting manifold is much smaller than the previous case, whereas the transient with respect to the temperature is larger due to the larger reaction rate during the transient period.

Figure 16 shows the dimension of the attracting manifold for CH_4/air mixtures along the trajectories. For the first row, the trajectory starts from a stoichiometric CH_4/air mixture. For the second row, the trajectory starts from the laminar flame results. As may be seen from

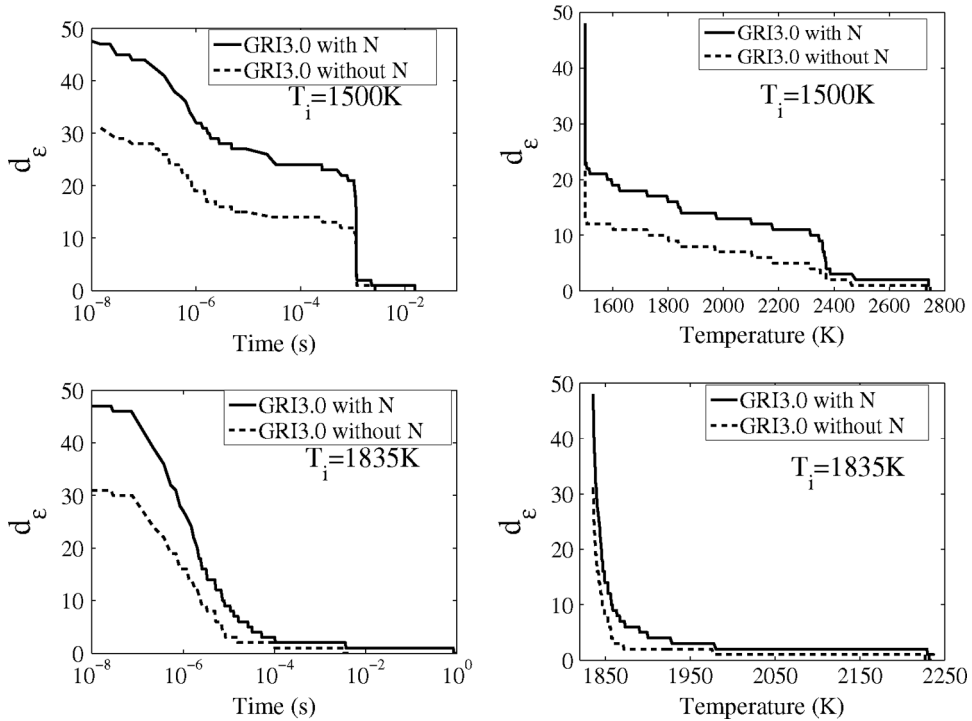


Figure 16. Dimension of the attracting manifold for CH_4/air against time and temperature along the trajectories. For the first row, the initial composition is chosen from $\text{CH}_4 - 2$ in table 1. For the second row, the initial composition is chosen from $\text{CH}_4 - 3$. The threshold ϵ is 0.01.

figure 16, for the first case the dimension of the attracting manifold quickly decreases to around 21 and 12 for the GRI3.0 with and without nitrogen chemistry, respectively; whereas for the second case the dimension of the attracting manifold quickly decreases to around 8 and 4 for the GRI3.0 with and without nitrogen chemistry. Therefore the behaviour is highly dependent on the location in the composition space. For these two cases, the dimension of the attracting manifold when starting from laminar flame results is much smaller than that when starting from the pure CH_4/air mixture. Nevertheless, after the initial transient, the dimension of the attracting manifolds for both cases is much smaller than the dimension of the full composition space. Also from figure 16, we see that nitrogen chemistry increases the dimension of the attracting manifold as expected (by about 4 to 9 after the initial transition): however, the number of dimensions increased is much smaller than the number of dimensions added to the full system by nitrogen chemistry. (Nitrogen chemistry adds 17 more dimensions to the system.)

It is informative to study the angle between the reaction rate vector and the ‘principal subspace’ along individual trajectories. The ‘principal subspace’ with fixed dimension d is the subspace spanned by the first d columns of the matrix $\tilde{\mathbf{U}}$ (see equation (37)), and is an approximation to the tangent space of the d -dimensional attracting manifold along the trajectory. If the identified ‘principal subspace’ is a good approximation to tangent space of the attracting manifold, the angle should remain small after the initial transient. Figure 17a shows the dimension of the attracting manifold for CH_4/air along the trajectory starting from pure stoichiometric CH_4/air mixture with initial temperature 1500 K. Figure 17c shows the angle between the reaction rate vector and the ‘principal subspace’ with dimension 3 and 6 along the trajectory, respectively. As may be seen from the figure, the angle is small after

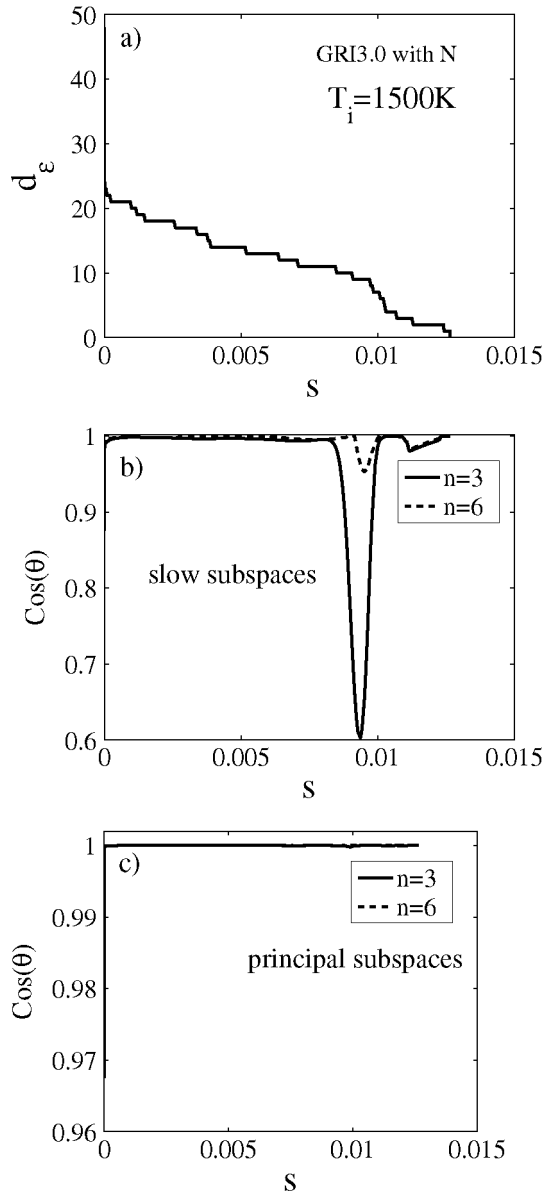


Figure 17. (a) Dimension of the attracting manifold for CH_4/air along the trajectory starting from a stoichiometric CH_4/air mixture with initial temperature 1500 K. (The threshold is $\epsilon = 0.01$.) (b) Angle between the reaction rate vector and the slow subspaces identified by the ILDM method (with dimension 3 and 6) along the trajectory. (c) Angle between the reaction rate vector and the 'principal subspaces' with the same dimensions along the trajectory.

the initial transient, which indicates that the reaction rate vector is aligned with the 'principal subspace'. For comparison, also shown in figure 17 is the angle between the reaction rate vector and the slow subspaces (identified by the ILDM method) with the same dimensions along the trajectory. Large angles occur after the initial transient, which indicates that the reaction rate vector is not aligned with the slow subspaces identified by the ILDM method based on the local Jacobian matrices. Another observation from figure 17 is that the reaction rate vector lies in a subspace of dimension much smaller than the dimension of the attracting manifold.

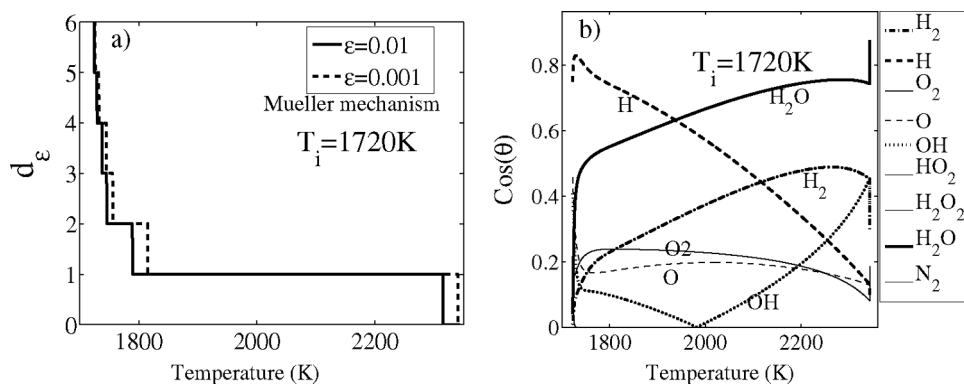


Figure 18. (a) Dimension of the attracting manifold for H_2/air against temperature along the trajectory starting from the initial condition $\text{H}_2 - 3$ in table 1. (b) Angle between the species vectors and the one-dimensional 'principal subspace' along the trajectory.

After the initial transient, the dimension of the attracting manifold is around 20 (figure 17a), whereas the reaction rate vector is in a 3-dimensional 'principal subspace' (figure 17c).

In simulations of combustion processes, it is convenient if the d -dimensional attracting manifold can be parameterized by d species. This requires that the mapping be one-to-one; and, to be well conditioned, it required that the largest angle between tangent space of the attracting manifold and the d species vectors be small (compared to $\pi/2$). For the chemical system, after determining the dimension of the attracting manifold and identifying the 'principal subspace' based on the sensitivity matrices, we can study the angle between the species vector and the 'principal subspace', and choose the species which have the smallest angle with the 'principal subspace' as the parameters. As shown in figure 18, after the initial transient, this chemical system approaches a one-dimensional attracting manifold and H_2O is a good parameter to parameterize this one-dimensional attracting manifold. (It is obvious in figure 14 that H_2O is a good parameter for the one-dimensional attracting manifold for the hydrogen systems.)

4.5 Discussion

The method proposed above can be used to determine the dimensionality of the attracting manifold along the reaction trajectory of a temporal chemical kinetic system starting from one particular initial composition. The method is sound no matter whether the initial composition is close to chemical equilibrium or not in the composition space. In the context of dimension reduction of chemistry over the whole realizable region, one can determine the minimum dimensionality of the attracting manifold required by using this method to perform dimension analysis for the trajectories starting from some edge in the realizable region. One such edge identified by Ren *et al.* in ref. [29] is the constrained equilibrium edge.

Also the method proposed is based on a homogeneous system without considering flow and molecular transport processes (i.e. isolating the chemical reaction from other processes). However, most interesting reacting flow problem involve the coupling of chemical kinetics with physical processes like flow and molecular transport. The physical processes can be viewed as disturbances of the chemical reaction system. In this case, besides the chemical time scales, the system has characteristic time scales of the physical processes. Of particular interest is the characteristic molecular diffusion time, which can serve as the threshold value to determine the minimum dimension of the attracting manifold required for the system.

5. Conclusion

In this work, we study the geometry of the reaction trajectories in the composition space for the autoignition of both H_2/air and CH_4/air mixtures. For these chemical systems, by studying the tangent bundle, we reveal that the dimension of the affine space containing the trajectory is much smaller than the dimension of the reactive subspace. For H_2/air with the Mueller mechanism, for all the cases studied, the dimension of the affine space is about 4, whereas the the dimension of the reactive subspace is 6. For CH_4/air , the dimensions of the affine spaces for GRI3.0 with and without nitrogen chemistry are about 11 and 8, respectively, whereas the dimensions of the reactive subspaces are 48 and 31, respectively. Large curvature along the trajectory is explained in terms of the chemical kinetics.

By studying the eigenvalues of the Jacobian along the trajectories in the composition space, we observe a wide range of time scales in the chemical dynamic system even at low temperatures, which provides direct support for the existence of low-dimensional attracting manifolds in the composition space.

The geometrical significance of sensitivity matrices is explored in this paper. Along the trajectory, at different times, in the reactive subspace, the initial infinitesimal ball centered at the initial point is mapped to a hyper-ellipsoid with the information of principal axes given by the sensitivity matrices. Based on the sensitivity matrices, a new method is proposed to determine the dimension of the attracting manifolds and identify the ‘principal subspace’ along the reaction trajectory. Compared with other existing methods that determine the local dimension of the attracting manifold for the chemical system, this new method is global in the sense that it is based on the sensitivity matrices instead of the local Jacobian matrices.

The method is applied to the autoignition of both H_2/air and CH_4/air mixtures. Studies also show that after the initial transient, the dimension of the attracting manifold is much smaller than the dimension of the full composition space. Considering nitrogen chemistry in the chemical dynamic system increases the dimension of the attracting manifold as expected (by about 4 to 9); however, the number of dimensions increased in the attracting manifold is smaller than the number of dimensions added to the system by nitrogen chemistry (which is 17). Moreover the behaviour is highly dependent on the location in the composition space.

Acknowledgments

This work is supported by Department of Energy, grant number DE-FG02-90ER14128.

References

- [1] Bodenstein, M. and Lind, S.C., 1906, Geschwindigkeit der Bildung des Bromwasserstoffs aus seinen Elementen. *Zeitschrift für Physikalische Chemie*, **57**, 168–175.
- [2] Smooke, M.D. (Ed.), 1991, *Reduced Kinetic Mechanisms and Asymptotic Approximations for Methane-Air Flames*, Vol. 384 (Berlin: Springer).
- [3] Keck, J.C. and Gillespie, D., 1971, Rate-controlled partial equilibrium method for treating reacting gas mixtures. *Combustion and Flame*, **17**, 237–241.
- [4] Keck, J.C., 1990, Rate-controlled constrained equilibrium theory of chemical reactions in complex systems. *Progress in Energy and Combustion Science*, **16**, 125–154.
- [5] Tang, Q. and Pope, S.B., 2002, Implementation of combustion chemistry by *in situ* adaptive tabulation of rate-controlled constrained equilibrium manifolds. *Proceedings of the Combustion Institute*, **29**, 1411–1417.
- [6] Maas, U. and Pope, S.B., 1992, Simplifying chemical-kinetics: intrinsic low-dimensional manifolds in composition space. *Combustion and Flame*, **88**, 239–264.
- [7] Pope, S.B. and Maas, U., 1993, Simplifying chemical kinetics: Trajectory-generated low-dimensional manifolds, FDA 93-11, Cornell University.

- [8] van Oijen, J.A. and de Goey, L.P.H., 2000, Modelling of premixed laminar flames using flamelet-generated manifolds. *Combustion Science and Technology*, **161**, 113–137.
- [9] Roussel, M.R. and Fraser, S.J., 1993, Global analysis of enzyme inhibition kinetics. *Journal of Physics and Chemistry*, **97**, 8316–8327.
- [10] Gorbunov, A.N. and Karlin, I.V., 2003, Method of invariant manifold for chemical kinetics. *Chemical Engineering Science*, **58**, 4751–4768.
- [11] Ren, Z. and Pope, S.B., 2005, Species reconstruction using pre-image curves. *Proceedings of the Combustion Institute*, **30**, 1293–1300.
- [12] Davis, M.J. and Skodje, R.T., 1999, Geometric investigation of low-dimensional manifolds in systems approaching equilibrium. *Journal of Chemistry and Physics*, **111**, 859–874.
- [13] Skodje, R.T. and Davis, M.J., 2001, Geometrical simplification of complex kinetic system. *Journal of Physics and Chemistry A*, **105**, 10356–10365.
- [14] Tomlin, A.S., Turányi, T. and Pilling, M.J., 1997, *Comprehensive Chemical Kinetics 35: Low-temperature Combustion and Autoignition* (Amsterdam: Elsevier).
- [15] Pope, S.B., 2004, Accessed compositions in turbulent reactive flows. *Flow, Turbulence and Combustion*, **72** (2–4), 219–243.
- [16] Deuffhard, P. and Heroth, J., 1996, Dynamic Dimension Reduction in ODE Models. In: Keil, F., Mackens, W., Vob, H., Werther, J. (Eds.), *Scientific Computing in Chemical Engineering* (Springer-Verlag), pp. 29–43.
- [17] Deuffhard, P., Heroth, J. and Maas, U., 1996, Towards dynamic dimension reduction in reactive flow problems. In: Proceedings of the 3rd Workshop on Modelling of Chemical Reaction Systems, Heidelberg.
- [18] Handrock-Meyer, S., Kalachev, L.V. and Schneider, K.R., 2001, A method to determine the dimension of long-time dynamics in multi-scale systems. *Journal of Mathematics and Chemistry*, **30**, 133–160.
- [19] Tomlin, A.S., Whitehouse, L., Lowe, R. and Pilling, M.J., 2002, Low-dimensional manifolds in tropospheric chemical systems. *Faraday Discussions*, **120**, 125–146.
- [20] Büki, A., Perger, T., Turányi, T. and Maas, U., 2002, Repro-modelling based generation of intrinsic low-dimensional manifolds. *Journal of Mathematics and Chemistry*, **31**, 345–362.
- [21] Rabitz, H., Kramer, M. and Dacol, D., 1983, Sensitivity analysis in chemical kinetics. *Annual Review of Physics and Chemistry*, **34**, 419–461.
- [22] Turányi, T., 1990, Sensitivity analysis of complex kinetic systems: tools and applications. *Journal of Mathematics and Chemistry*, **5**, 203–248.
- [23] ADIFOR 2.0, Automatic Differentiation of Fortran <http://www-unix.mcs.anl.gov/autodiff/ADIFOR/>
- [24] Caracotsios, M. and Stewart, W.E. 1985, Sensitivity analysis of initial value problems with mixed ODEs and Algebraic equations. *Computers and Chemical Engineering*, **9**, 359–365.
- [25] Mueller, M.A., Kim, T.J., Yetter, R.A. and Dryer, F.L., 1999, Flow reactor studies and kinetic modeling of the H₂/O₂ reaction. *International Journal of Chemical Kinetics*, **31**, 113–125.
- [26] Li, J., Zhao, Z., Kazakov, A. and Dryer, F.L., 2003, An updated comprehensive kinetic model for H₂ combustion. Fall Technical Meeting of the Eastern States Section of the Combustion Institute, Penn State University, University Park, PA, October 26–29.
- [27] Smith, G.P., Golden, D.M., Frenklach, M., Moriarty, N.W., Eiteneer, B., Goldenberg, M., Bowman, C.T., Hanson, R.K., Song, S., Gardiner, W.C., Lissianski, V.V. and Qin, Z., http://www.me.berkeley.edu/gri_mech/.
- [28] Warnatz, J., Maas, U. and Dibble, R.W., 1999, *Combustion: Physical and Chemical Fundamentals, Modeling and Simulation, Experiments, Pollutant Formation* (Berlin: Springer).
- [29] Ren, Z., Pope, S.B., Vladimirov, A. and Guckenheimer, J.M., The invariant constrained equilibrium edge preimage curve method for the dimension reduction of chemical kinetics. *Journal of Chemistry and Physics* **124**, 114111.